

Vortex-phase filtering technique for extracting spatial information from unresolved sources

Garreth J. Ruane, Prachyathit Kanburapa, Jiaxuan Han, and Grover A. Swartzlander, Jr.*

*Chester F. Carlson Center for Imaging Science, Rochester Institute of Technology,
54 Lomb Memorial Drive, Rochester, NY 14623, USA*

A white light vortex coronagraph was used to experimentally achieve sub-resolution detection. The angular location of the centroid, γ , and the angular extent of circular pinhole sources, Θ , were measured to within errors of $\gamma = \pm 0.015 \lambda/D$ and $\Theta = \pm 0.026 \lambda/D$. This technique has two advantages over conventional imaging: simple power measurements are made and shorter exposure times are required to achieve a sufficient signal-to-noise ratio.

I. INTRODUCTION

The spatial resolution of an imaging system is fundamentally limited by the wave nature of light. Although low f -number optical elements reduce undesirable diffraction effects, fabricating extremely large optics with strong curvature is impractical. However, optical pre-detection processing techniques may be employed to circumvent conventional resolution criteria, including magnitude and/or phase filtering [1, 2]. Moreover, non-imaging sensors as described here may be advantageous for obtaining specific source information otherwise obscured in images. We demonstrate a vortex-phase filtering technique for extracting the centroid and spatial extent of an unresolved source distribution [3]. Spatially integrated power measurements provide sub-resolution structure information akin to radial moments of the source (e.g. the variance). This approach may be suitable for high-precision

tracking and monitoring of unresolved targets, such as near earth objects or small satellites.

Applications of vortex phase elements span many areas of imaging science including optical spatial filtering [4], phase contrast microscopy [5], and high-contrast astronomical imaging [6, 7]. The latter makes use of an optical vortex coronagraph (OVC). The OVC is a Fourier filtering instrument wherein a focal plane vortex phase element acts to spatially separate light originating from a distant point source that coincides with the optical axis from nearby off-axis sources. Consequently, the OVC is adept at small-angle high-contrast astronomical observations, such as directly imaging exoplanets [8].

The optical design demonstrated here is adopted from a recently introduced broadband scalar OVC [9–11]. This scheme incorporates a computer generated vortex hologram and a complementary dispersion compensating diffraction grating in order to realize a vortex-phase filtering instrument that may be used with white

* Corresponding author: grover.swartzlander@gmail.com

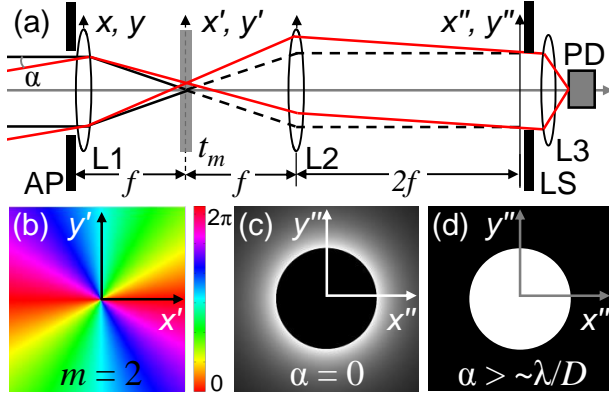


FIG. 1. (a) Schematic of an OVC with lens L1 located at entrance aperture AP, vortex phase element with transmission $t_m = \exp(im\theta')$, and field lens L2. The geometric exit pupil is located at the x'', y'' plane, where the Lyot stop (LS) truncates the field. The spatially integrated power transmitted through the LS is recorded by a photo detector (PD). (b) Phase profile of vortex phase mask with transmission $\exp(i2\theta')$. (c) On-axis coherent light ($\alpha = 0$) is diffracted outside of the geometric exit pupil ($m = 2$ case shown). (d) Tilted plane waves at the aperture form an approximate image of the entrance pupil at the x'', y'' plane.

light. We demonstrate using the broadband scalar OVC to determine the spatial extent of unresolved sources in the laboratory.

II. BROADBAND VORTEX-PHASE FILTERING

The standard layout of an OVC is a $4f$ lens system [see Fig. 1]. Lens L1, located at the entrance aperture (AP), focuses light onto a vortex phase element with transmission $t_m = \exp(im\theta')$, where m is a nonzero integer and θ' is the azimuth in the x', y' plane [see Fig. 1(b)].

For even values of m , all irradiance from a point source whose focal spot is centered on the phase singularity diffracts outside of the geometric image of AP. The field at the exit pupil plane may be written in polar coordinates as

$$U_m(r'', \theta'') = \begin{cases} \Lambda_m \frac{R}{r''} Z_n^1\left(\frac{R}{r''}\right), & r'' > R \\ 0, & r'' < R \end{cases}, \quad (1)$$

where m is an even nonzero integer, R is the radius of AP, $n = |m| - 1$, $\Lambda_m = \exp(im\theta'')$, and $Z_n^1(R/r'')$ are the radial Zernike polynomials [12]. For $m = 2$, the exterior field is $U_2(r'', \theta'') = (R/r'')^2 \exp(i2\theta'')$ [see Fig. 1(c)]. On the other hand, the focal spot due to an off-axis source is displaced away from the phase singularity in the x', y' plane. Consequently, the vortex phase element has little effect on the image of AP [see Fig. 1(d)]. By placing a second aperture at the x'', y'' plane, known in coronagraphy as the Lyot stop (LS), light originating from the on-axis source is cancelled while off-axis sources are preserved. The radius of the LS, must be less than that of AP to reject all of the light from an on-axis source. Here we shall assume $R_{LS} = R/2$. Fig. 2 shows the power transmitted through the LS from a distant point source, P_m , displaced from the optical axis by angle α . In the $m = 2$ case, the source is attenuated by $\sim 50\%$ when $\alpha = \lambda/D$, where λ is the wavelength and $D = 2R$. Meanwhile, P_m falls off asymptotically as α approaches zero. Systems with higher m values reject more light from off-axis sources [6, 7].

The application described here requires high

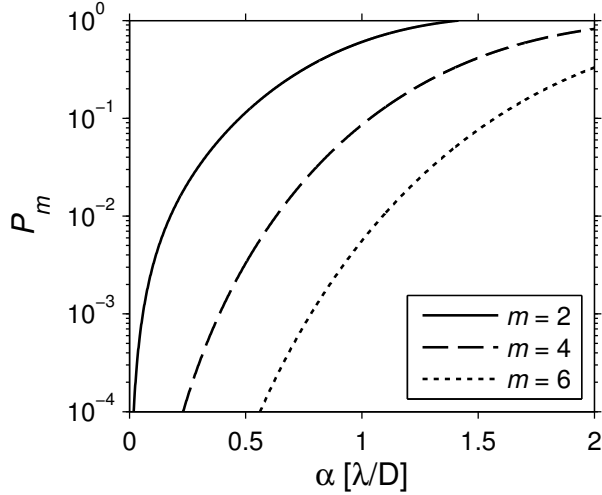


FIG. 2. The power transmitted through the LS due to a distant point source displaced from the optical axis by angle α in units of the resolution angle λ/D .

precision vortex elements such as a spiral phase plate produced via electron beam lithography [13], subwavelength diffraction gratings [6, 14, 15], liquid crystal elements [16, 17], or photonic crystal elements [18]. The spiral phase plate operates at a single wavelength, which may not be practical for white light systems. The other approaches have reported bandwidths as large as $\lambda/\Delta\lambda = 20\%$. Here we employ a vortex hologram (VH) and dispersion compensation to achieve a bandwidth of 50%. The VH is a holographic representation of the interference pattern between a vortex and a plane wave [19, 20]. A VH with topological charge $m = 2$ [see Fig. 3] provides the desired transmission function $t_2 = \exp(i2\theta')$ in the first diffracted order. Much like conventional gratings, the beam emergence angle is wavelength dependent. Thus, a complementary diffraction grating (DG) may be used to

compensate for chromatic dispersion while maintaining the vortex phase [21, 22]. The broadband performance of the holographic approach compares well with other high-precision vortex phase elements [9–11]. However, sufficient contrast performance for exoplanet imaging beyond $\lambda/\Delta\lambda = 20\%$ has not yet been demonstrated.

The operation of the holographic OVC [see Fig. 4] is similar to that of the schematic in Fig. 1, but the entrance pupil plane is reimaged twice. The VH shown in Fig. 3(b) is placed at the first focal plane of the imaging system. The emerging light in the first order has the desired transmission and is dispersed laterally with wavelength [see Fig 4(b)]. The focal spot is reimaged onto a diffraction grating (DG) whose pitch matches that of the VH. The second grating compensates for the dispersion introduced by the VH in the first diffracted order without modifying the vortex phase. The result is a broadband OVC wherein the field patterns at the final pupil plane are given by Eq. (1).

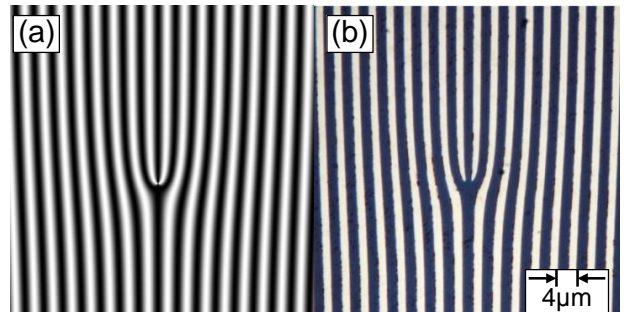


FIG. 3. (a) Theoretical interference pattern between a plane wave and a charge $m = 2$ vortex. (b) Binary amplitude grating fabricated by laser lithography with 250 line pairs per mm ($4\mu\text{m}$ pitch).

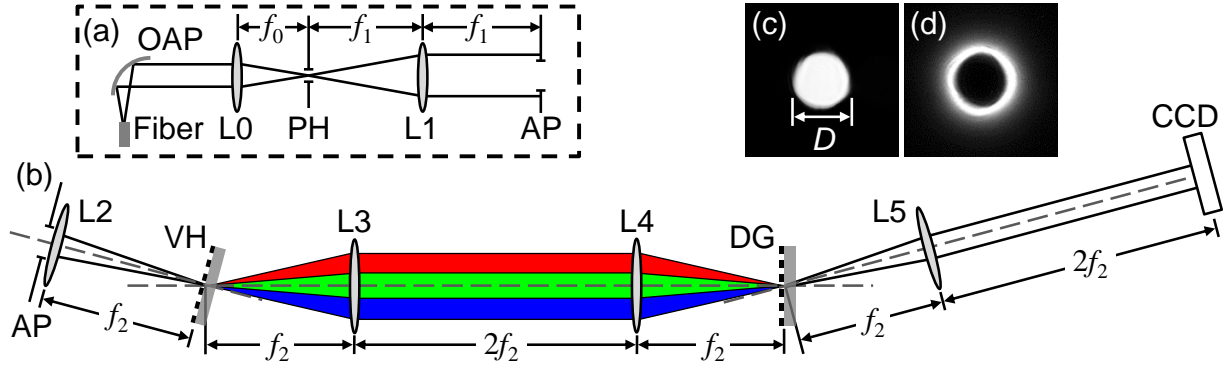


FIG. 4. Experimental implementation of a broadband holographic OVC. (a) White light is launched from a fiber, collimated by an off-axis parabolic mirror OAP, and focused by lens L0 ($f_0 = 30$ mm) on to a small pinhole (PH). Lens L1 ($f_1 = 30$ mm or 100 mm) forms the Fourier transform of PH at aperture AP ($D = 0.5$ mm) to simulate a distant point source. Quasi-plane waves enter the OVC at AP. (b) Light that transmits through AP is focused by lens L2 onto vortex hologram VH [see Fig. 3(b)], which impresses an $m = 2$ vortex phase profile on the first diffracted order. Lenses L3 and L4 reimagine the focal spot at diffraction grating DG with pitch equal to that of the VH ($4 \mu\text{m}$). Hence, light that emerges in the first diffracted order from DG is dispersion compensated. Lens L5 forms the exit pupil at the CCD. Lenses L2, L3, L4, and L5 have focal length $f_2 = 300$ mm. (c)-(d) Measured irradiance at the CCD with $5 \mu\text{m}$ diameter pinhole and $f_1 = 30$ mm. (c) If the pinhole is displaced from the optical axis, an approximate image of the entrance pupil appears at the CCD. (d) In the case where the pinhole source coincides with the optical axis, most of the light is relocated outside of the geometric exit pupil.

To demonstrate the optical system illustrated in Fig. 4 in the laboratory, white light (400 nm to 700 nm) from a fiber-coupled plasma source is collimated by an off-axis parabolic mirror OAP and is subsequently focused onto a small pinhole by lens L0 (*diameter* = 25.4 mm, $f_0 = 30$ mm). The pinhole size may vary from $5 \mu\text{m}$ to $25 \mu\text{m}$. Lens L1 (*diameter* = 25.4 mm, $f_1 = 30$ mm or 100 mm) collimates the transmitted light such that the pinhole simulates an unresolved source. The OVC entrance pupil is formed by aperture AP with diameter $D = 0.5$ mm. AP is immediately followed by focusing lens L2 (*diameter* = 25.4 mm, $f_2 = 300$ mm). An evenly illuminated entrance pupil forms an Airy disk that is centered on the central dislocation of a VH with $4 \mu\text{m}$ pitch. The VH fabricated for this demonstration approximates the forked interference pattern with a binary amplitude grating printed by a laser lithographic technique at $0.6 \mu\text{m}$ resolution on a 2 mm thick fused silica plate [see Fig 3(b)]. We approach a point phase singularity by ensuring the central feature is much smaller than the focal spot size. Specifically, the central lobe of the Airy disk covers approximately 256 and 146 line pairs for the red and blue light,

respectively. The first diffracted order, containing an $m = 2$ vortex, passes through field lens L3 (*diameter* = 50.8 mm, $f_2 = 300$ mm) to form a laterally dispersed pattern at the first pupil plane, where the field is imaged onto a DG with $4\ \mu\text{m}$ pitch by lens L4 (*diameter* = 50.8 mm, $f_2 = 300$ mm). The recombined beam passes through field lens L5 (*diameter* = 25.4 mm, $f_2 = 300$ mm) and forms the final pupil plane at the CCD. The image of the entrance aperture appears if the pinhole is displaced from the optical axis [see Fig. 4(c)]. However, if the center of the pinhole is aligned with the optical axis, the light is relocated outside of the geometric image of AP [see Fig. 4(d)]. The transmission of the OVC optics (from AP to the CCD) is 0.56%. We achieve a relative on-axis suppression of 2×10^{-4} with a pinhole source whose angular extent is $0.05\ \lambda/D$ over a $\lambda/\Delta\lambda = 50\%$ passband (300 nm band centered at 550 nm). The suppression is reported relative to the $m = 0$ case and was calculated from the signal present in the LS region of the CCD image with the background signal removed. The imperfect source cancellation is due, in part, to the extended size of the pinhole source.

III. SUB-RESOLUTION MEASUREMENTS

Although the structure of an unresolved source distribution is obscured in conventional images, a non-imaging vortex-phase filtering ap-

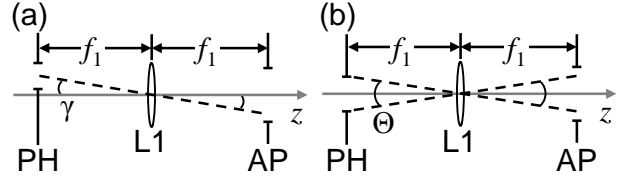


FIG. 5. Diagram of pinhole source PH [see Fig. 4(a)] whose centroid is (a) misaligned and (b) aligned with the optical axis. The angles γ and Θ refer to the angular displacement of the source centroid and angular extent of the pinhole source, respectively. Lens L1 forms the Fourier transform of the source at AP.

proach may be employed to extract spatial information. An ideal OVC removes the zero spatial frequency component of a field distribution with constant irradiance across the aperture. In other words, the OVC completely cancels a distant on-axis point source. Meanwhile, unresolved point sources that are displaced from the optical axis are only partially suppressed. Since small differences in source position yield a large transmission response, the OVC is uniquely sensitive to extended, yet unresolvable, source distributions. In the scheme employed here, the centroid and angular extent of a spatially incoherent distribution is determined. We demonstrate the $m = 2$ case; however, any nonzero even value of m may be used to make similar measurements.

A. Locating the centroid

The centroid of an unresolved source distribution is accurately aligned with the optical axis by locating the source position that corresponds to the minimum transmitted power through the

LS, T_m . Using the experimental arrangement described in Fig. 4, we measured T_2 in the laboratory for pinhole sources with various effective angular extents Θ as a function of the angular position of the source centroid γ [see Fig. 5]. For experimental convenience, we chose to displace the VH transverse to the optical axis rather than the pinhole [see Fig. 4(b)]. Shifting the center of the VH with respect to the focal spot is theoretically equivalent to displacing the pinhole from the optical axis. The values of T_2 were calculated from the CCD images at the exit pupil with the background signal removed. The angular extent of the source Θ was set by varying both the diameter of the pinhole D_{PH} and the value of f_1 . Fig. 6 shows the results for three represen-

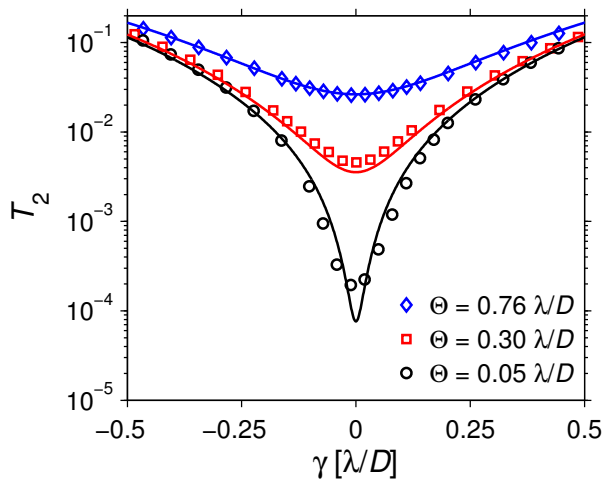


FIG. 6. Measured power in the LS region of the CCD image due to a circular source with angular extent Θ as a function of the angular displacement γ . The theoretical results (solid lines) are included for comparison. The power is normalized to the $m = 0$ case and a central wavelength of $\lambda = 550$ nm is assumed.

tative sources. The results compare well with the expected values and verify that the system has a steep power response to small angular displacements below the diffraction limit. The centroid of the pinhole sources was located within $\pm 0.015 \lambda/D$. In the case where the centroid is aligned with the optical axis (i.e. $\gamma = 0$), a nonzero signal is indicative of the angular extent of the source, as described below [3].

B. Determining spatial extent

If the centroid of the source is aligned with the optical axis, the effective angular extent of the source distribution may be deduced from the value of T_m . A simple measure of the source size is the power ratio

$$\eta_m = \frac{T_m}{T_0} \Big|_{\gamma=0}. \quad (2)$$

The transmission in the $m = 0$ case T_0 may be obtained by measuring the power in the central diffraction order from the VH or with the source substantially displaced from the optical axis. In the laboratory, we measure for ten values of Θ (five pinhole diameters: $D_{PH} = 5, 10, 15, 20, 25 \mu\text{m}$ and two lens L1 focal lengths: $f_1 = 30$ mm, 100 mm). The experimental results, shown in Fig. 7, follow the expected trend obtained numerically, which in practice may serve as a “look up table” for the estimated source size. The measured values for Θ have a root-mean-square deviation of $0.026 \lambda/D$. Discrepancies are due to misalignment and aberrations.

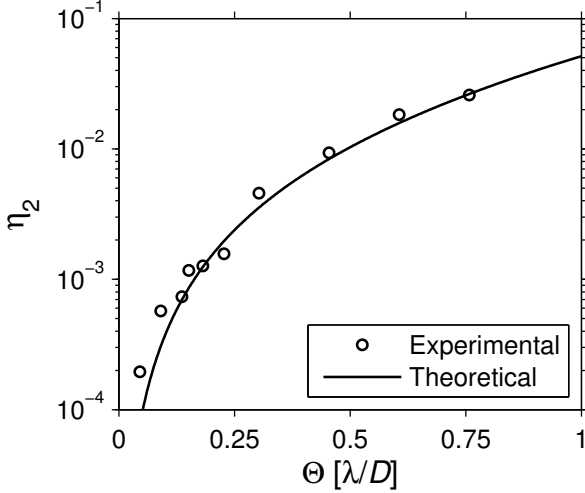


FIG. 7. Relative power in the LS region of the CCD for ten different effective angular extents Θ with the source centroid located on the optical axis (i.e. $\gamma = 0$). The power is normalized to the $m = 0$ case and a central wavelength of $\lambda = 550$ nm is assumed.

tions in the optical system.

In the limiting case where Θ approaches zero with respect to the angular resolution of the system, the values of η_m have a more familiar meaning. Assuming a localized spatially incoherent source,

$$\eta_m = \frac{1}{T_0} \int P_m(\alpha) I(\alpha) \sin(\alpha) d\alpha, \quad (3)$$

where $I(\alpha)$ is the irradiance distribution of the source. The power response due to extremely small displacements from the optical axis (i.e. $\alpha \ll \lambda/D$) is $P_m \propto \alpha^{|m|}$ [23]. Thus, the expression in Eq. (3) simplifies to the radial moments of the source distribution

$$\eta_m = \frac{1}{T_0} \int \alpha^{|m|} I(\alpha) \sin(\alpha) d\alpha. \quad (4)$$

It is possible to obtain improved spatial information by measuring several even order moments

of the source. However, higher values of m yield substantially lower signal. Likewise, more power is rejected in the case of a spatially coherent source. Although it is feasible to measure the angular extent of a coherent source with an OVC, this technique is best suited for spatially incoherent sources.

C. Noise considerations

The main advantage of the vortex filtering approach to sub-resolution detection is that shorter exposure times may be required compared to conventional imaging systems. Suppose we wish to determine the distance between two point sources. We choose the exposure time Δt_m such that a signal-to-noise ratio $SNR_m = 5$ is achieved with an OVC as shown in Fig. 1. The

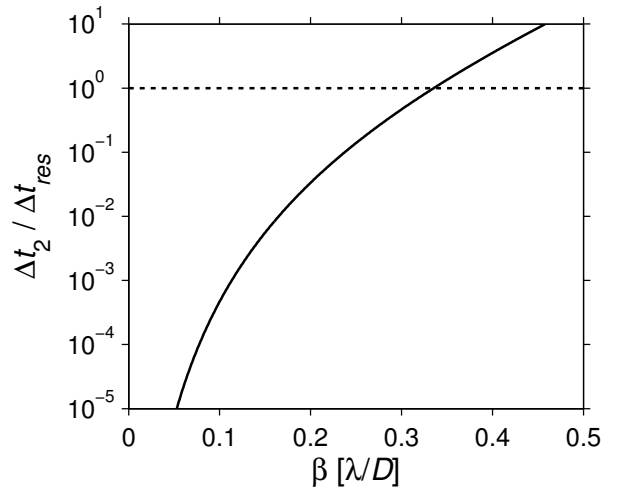


FIG. 8. The theoretical exposure time ratio to achieve $SNR = 5$ with the OVC system Δt_2 relative to the exposure required to distinguish the point sources with a conventional diffraction-limited imaging system as described in [24].

signal at the aperture is $S_0 = S_m/\eta_m$, where S_m is the detected signal. Assuming the system is shot noise limited, the corresponding signal-to-noise ratio is $SNR_0 = SNR_m/\eta_m^{-1/2}$. For a conventional diffraction-limited imaging system, on the other hand, the achievable resolution is restricted by the SNR . The SNR per pixel required to distinguish two point sources separated by angle β is approximately

$$SNR_\beta = \frac{1}{N^2} \left[\frac{6.12}{\beta^4} - \frac{16.38}{\beta^2} + 16.7 \right], \quad (5)$$

where N^2 is the number of pixels and β is in units of λ/D [24]. Fig. 8 shows the relative exposure time required to detect the source separation using an $m = 2$ OVC system. The vortex filtering approach requires substantially lower exposure times for $\beta < \sim 1/3 \lambda/D$. In practice, further improvements are possible since using single pixel photo detectors may mitigate other noise contributions of CCD or CMOS sensors, such as read noise and dark current.

IV. CONCLUSION

A vortex-phase filtering technique for sub-resolution information extraction has been demonstrated. This approach allows for precision pinpointing of the centroid of an unresolved source and yields quantitative measurements of the angular extent with white light ($\lambda/\Delta\lambda = 50\%$). Spatial information is deduced from simple pupil plane power measurements at the exit pupil of a vortex coronagraph. Prior knowledge of the source structure is not required. What is more, sub-resolution detection may be performed with considerably lower exposure times than conventional imaging.

ACKNOWLEDGMENTS

We acknowledge the Cornell Nanofabrication Facility and Sydor Optics for fabricating the vortex holograms used in this study. We also thank Mr. Thomas Grimsley, Dr. Alan Raisanen, and Dr. Stefan Preble from RIT for discussion regarding fabrication processes. This work was supported by the U.S. Army Research Office under grant number W911NF1110333-60577PH.

[1] H. Osterberg and J. E. Wilkins, Jr., "The Resolving Power of a Coated Objective," *J. Opt. Soc. Am.* **39**, 553-557 (1949).
 [2] G. Toraldo Di Francia, "Super-gain antennas and optical resolving power," *Il Nuovo Cimento Suppl.* **9**, 426-438 (1952).

[3] G. A. Swartzlander, Jr., "Obtaining spatial information from an extremely unresolved source," *Opt. Lett.* **36**, 4731-4733 (2011).
 [4] S. N. Khonina, V. V. Kotlyar, M. V. Shinkaryev, V. A. Soifer, and G. V. Uspleniev, "The Phase Rotor Filter," *J. Mod. Opt.* **39**, 1147-1154

- (1992).
- [5] S. Furbapter, A. Jesacher, S. Bernet, and M. Ritsch-Marte, "Spiral phase contrast imaging in microscopy," *Opt. Express* **13**, 689-694 (2005).
- [6] D. Mawet, P. Riaud, O. Absil, and J. Surdej, "Annular groove phase mask coronagraph," *Astrophys. J.* **633**, 1191-1200 (2005).
- [7] G. Foo, D. M. Palacios, and G. A. Swartzlander, Jr., "Optical vortex coronagraph," *Opt. Lett.* **30**, 3308-3310 (2005).
- [8] E. Serabyn, D. Mawet, and R. Burruss, "An image of an exoplanet separated by two diffraction beamwidths from a star," *Nature* **464**, 1018-1020 (2010).
- [9] P. Kanburapa and G. A. Swartzlander, Jr., "White-Light Optical Vortex Coronagraph," in *OSA Technical Digest (online)* (Optical Society of America, 2012), p. FTh4E.2.
- [10] P. Kanburapa, "White-light Optical Vortex Coronagraph," M.S. thesis, Rochester Institute of Technology (2012).
- [11] R. Errmann, S. Minardi, and T. Pertsch, "A broad-band scalar vortex coronagraph," *Mon. Not. R. Astron. Soc.* **stt1317** (2013).
- [12] A. Carlotti, G. Ricort, and C. Aime, "Phase mask coronagraphy using a Mach-Zehnder interferometer," *Astron. Astrophys.* **504**, 663-671 (2009).
- [13] G. A. Swartzlander, Jr., E. L. Ford, R. S. Abdul-Malik, L. M. Close, M. A. Peters, D. M. Palacios, and D. W. Wilson, "Astronomical demonstration of an optical vortex coronagraph," *Opt. Express* **16**, 10200-10207 (2008).
- [14] Z. Bomzon, V. Kleiner, and E. Hasman, "Pancharatnam-Berry phase in space-variant polarization-state manipulations with subwavelength gratings," *Opt. Lett.* **26**, 1424-1426 (2001).
- [15] C. Delacroix, O. Absil, P. Forsberg, D. Mawet, V. Christiaens, M. Karlsson, A. Boccaletti, P. Baudoz, M. Kuittinen, I. Vartiainen, J. Surdej, and S. Habraken, "Laboratory demonstration of a mid-infrared AGPM vector vortex coronagraph," *Astron. Astrophys.* **553**, A98 (2013).
- [16] L. Marrucci, C. Manzo, and D. Paparo, "Optical spin-to-orbital angular momentum conversion in inhomogeneous anisotropic media," *Phys. Rev. Lett.* **96**, 163905 (2006).
- [17] D. Mawet, E. Serabyn, K. Liewer, C. Hanot, S. McEldowney, D. Shemo, and N. O'Brien, "Optical vectorial vortex coronagraphs using liquid crystal polymers: theory, manufacturing and laboratory demonstration," *Opt. Express* **17**, 1902-1918 (2009).
- [18] N. Murakami, S. Hamaguchi, M. Sakamoto, R. Fukumoto, A. Ise, K. Oka, N. Baba, and M. Tamura, "Design and laboratory demonstration of an achromatic vector vortex coronagraph," *Opt. Express* **21**, 7400-7410 (2013).
- [19] V. Y. Bazhenov, M. V. Vasnetsov, and M. S. Soskin, "Laser beams with screw dislocations in their wavefronts," *Pisma Zh. Eksp. Teor. Fiz.* **52**, 1037-1039 (1990) [*JETP Lett.* **52**, 429-431 (1990)].
- [20] N. R. Heckenberg, R. McDuff, C. P. Smith, and A. G. White, "Generation of optical phase singularities by computer-generated holograms," *Opt. Lett.* **17**, 221-223 (1992).
- [21] J. Leach and M. J. Padgett, "Observation of chromatic effects near a white-light vortex," *New J. Phys.* **5**, 154-154 (2003).
- [22] I. G. Mariyenko, J. Strohaber, and C. J. G. J. Uiterwaal, "Creation of optical vortices in femtosecond pulses," *Opt. Express* **13**, 7599-7608

- (2005).
- [23] C. Jenkins, "Optical vortex coronagraphs on ground-based telescopes," *Mon. Not. R. Astron. Soc.* **384**, 515-524 (2008).
- [24] M. Shahram and P. Milanfar, "Statistical analysis of achievable resolution in incoherent imaging," *Proc. SPIE* **5204**, 1-9 (2003).